Spatial Coherence of a Polariton Condensate

Hui Deng,[1,*] Glenn S. Solomon,[2] Rudolf Hey,[3] Klaus H. Ploog,[3] and Yoshihisa Yamamoto[1,4]

[1]*Edward L. Ginzton Laboratory, Stanford University, Stanford, California 94305, USA*
[2]*National Institute of Standards and Technology, Physics Laboratory,*
100 Bureau Drive, MS 8423, Gaithersburg, Maryland 20899, USA
[3]*Paul-Drude-Institut für Festkörperelektronik, Hausvogteiplatz 5-7, D-10117 Berlin, Germany*
[4]*National Institute of Informatics, Tokyo, Japan*

We perform Young's double-slit experiment to study the spatial coherence properties of a two-dimensional dynamic condensate of semiconductor microcavity polaritons. The coherence length of the system is measured as a function of the pump rate, which confirms a spontaneous buildup of macroscopic coherence in the condensed phase. An independent measurement reveals that the position and momentum uncertainty product of the condensate is close to the Heisenberg limit. An experimental realization of such a minimum uncertainty wave packet of the polariton condensate opens a door to coherent matter-wave phenomena such as Josephson oscillation, superfluidity, and solitons in solid state condensate systems.

Simple, yet profoundly connected to the foundation of quantum physics, Young's double-slit experiment has been a benchmark demonstration of macroscopic spatial coherence—off-diagonal long range order (ODLRO) of a macroscopic number of particles [1]—in Bose-Einstein condensation (BEC) of cold atoms [2–4]. Recently, a similar phase transition has been reported for the lower branch of exciton-polaritons (LPs) in planar semiconductor microcavities [5–12], and supporting theoretical frameworks have been developed [13–20]. Interestingly, LPs are free particles in a two-dimensional (2D) system where genuine BEC exists only at zero temperature in the thermodynamic limit [21,22]. A quasi-BEC can be defined for a 2D system of a finite size if a macroscopic number of particles occupy a single ground state and if an ODLRO is established throughout the system [23,24]. Yet in the LP experiments to date, the system size is ambiguously defined by the spot size of the pump laser, and there is no quantitative study of the relation between the size and the coherence length of a condensate [10,11]. In this work, we perform Young's double-slit experiment on a LP gas to measure its spatial coherence properties across the phase transition, and compare the measured coherence length with the condensate size. We also measure the position-momentum uncertainty product of the condensate and compare it to the Heisenberg limit.

A sketch of the setup is shown in Fig. 1. The microcavity sample is first magnified by a factor of 37.5 and imaged to a plane A, which is in turn imaged by a lens II to a charge-coupled device (CCD) at plane C for measurement of spatial distribution. For the double-slit experiment, we insert a pair of rectangular slits at plane A, and move the lens II such that the image of plane A (denoted by plane B) is a distance D behind plane C. Effectively, we observe on the CCD the interference pattern of the LP emission passing through the double slit. In our experiment, $D = 6.7$ cm,

the width of the slit image at plane B is $\delta = 53$ μm, and the average wavelength of the LP emission is $\lambda \sim 778.5$ nm. Correspondingly, the Fresnel number $\frac{\delta^2}{D\lambda} = 0.05 \ll 1$, thus the far-field condition is satisfied at plane C. When mapped onto the sample surface, the slit width seen by the LPs is $\Delta r \approx 0.5$ μm, which is less than the intrinsic coherence length $\xi_0 \sim 1$ μm of a single LP [25], and much less than the LP system size of 5–10 μm. Hence neglecting the variation in LP distribution within each slit, we obtain the intensity distribution on the CCD camera [26]:

$$I(x) = I_1(x) + I_2(x)$$
$$+ g^{(1)}(|r_1 - r_2|)2\sqrt{I_1(x)I_2(x)}\cos(\phi(x) + \phi_{12}),$$
$$I_i(x) = |E(r_i)|^2\mathrm{sinc}\left(\frac{x - x_0 \pm d/2}{X}\right), \qquad \phi(x) = \frac{2(x - x_0)}{X_c},$$
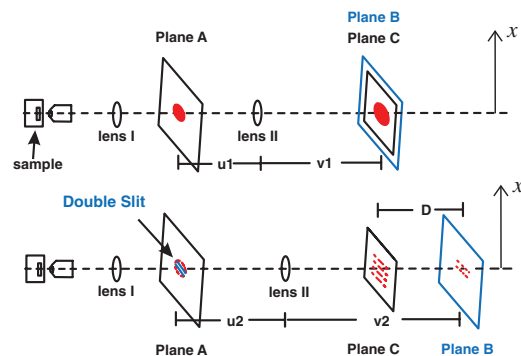$$X = \frac{2D}{k_{\mathrm{tot}}\delta}, \qquad X_c = \frac{2D}{k_{\mathrm{tot}}d}. \tag{1}$$

FIG. 1 (color). A sketch of the double-slit experiment setup. Upper: the LP spatial distribution is imaged to a CCD at plane C. Lower: a double-slit is inserted at plane A and imaged by lens II to a virtual plane B. The CCD at plane C, a distance D from plane B, captures the double-slit interference pattern.

The subscript $i = 1, 2$ denotes the slit number. r_i are the x coordinates of the slits on plane B (Fig. 1), x is the x coordinate on plane C, x_0 is the center of the double slit on plane C, $E(r_i)$ is the LP field amplitude at slit i, k_{tot} is the free space average wave number of the LP emission, and d is the separation between the images of the two slits at plane B. I_i is the intensity distribution if only slit i is open. ϕ_{12} is a fixed phase difference of LPs between the two slits. $\phi(x)$ is a varying phase close to the path length difference from the two slits, giving rise to a cosine modulation on the far-field intensity distribution. After proper normalization, the amplitude of the cosine modulation equals the first-order coherence function $g^{(1)}(r = |r_1 - r_2|)$. Using six sets of double-slit with varying slit separations r, we measured $g^{(1)}(r)$ from 1.3 μm, close to the intrinsic coherence length of a single LP, up to 8 μm, close to the LP system size. By varying the pumping intensity, we studied the characteristics of $g^{(1)}(r)$ across the phase transition.

The sample we investigated has a $\lambda/2$ GaAs cavity sandwiched between $Ga_{0.865}Al_{0.135}As/AlAs$ distributed Bragg reflectors. Three stacks of quantum wells (QWs) are placed at the central three antinodes of the microcavity, each stack consisting of four 6.8 nm-wide GaAs QWs separated by 2.7 nm-wide AlAs barriers. We pump the sample with linearly polarized picosecond mode-locked Ti:sapphire laser. At an incidence angle of 50° from the sample growth direction, the laser is resonant with the excitonlike LP modes. The sample is kept at $T_{\text{lattice}} \approx$ 4 K. The cavity-photon energy at zero in-plane wave number is ~7 meV above the bare QW exciton resonance, corresponding to an optimal detuning for thermal-equilibrium condensation of the LPs [12]. The threshold pumping density is $P_{th} \sim 300$ W/cm^2 [27].

A typical interference pattern observed at a pump rate above the condensation threshold is shown in Fig. 2(a). Distinct interference fringes are readily observed imposed on a sinc function distribution. To obtain $g^{(1)}(r)$, we integrate over a narrow strip along the y axis and fit it with Eq. (1). $g^{(1)}$, ϕ_{12}, $|E_1|$, and $|E_2|$ are free fitting parameters, while x_0, d, X, and X_c are estimated from experimental parameters with a 10% allowed variation. As shown in Fig. 2(b), Eq. (1) fits the data very well for $P > P_{th}$. At $P < P_{th}$, the interference patterns are barely observable or nonexisting; one example is given in Fig. 2(c).

In Fig. 3(a) we show the increase of $g^{(1)}(r)$ with P/P_{th} for a few slit separations r. A salient feature in Fig. 3(a) is that there is a jump in $g^{(1)}(r)$ when the pump rate is increased above a condensation threshold, even at r up to
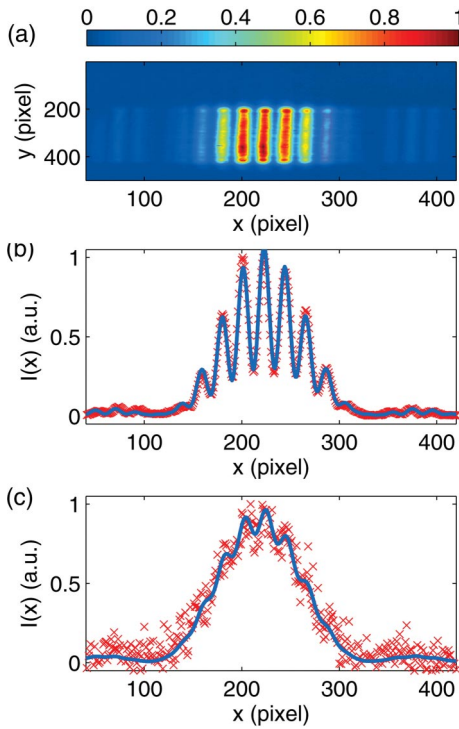

FIG. 2 (color). (a) Raw image of the interference pattern, slit separation $r = 2.7$ μm, $P/P_{th} = 7$. (b) Measured (symbols) intensity $I(x)$ for $r = 2.7$ μm, $P/P_{th} = 6.7$ and fitting by Eq. (1). Fitted $g^{(1)}(r) = 0.560 \pm 0.006$. (c) Same as (b), for $r = 2.7$ μm, $P/P_{th} = 0.5$, and $g^{(1)}(r) = 0.09 \pm 0.02$.
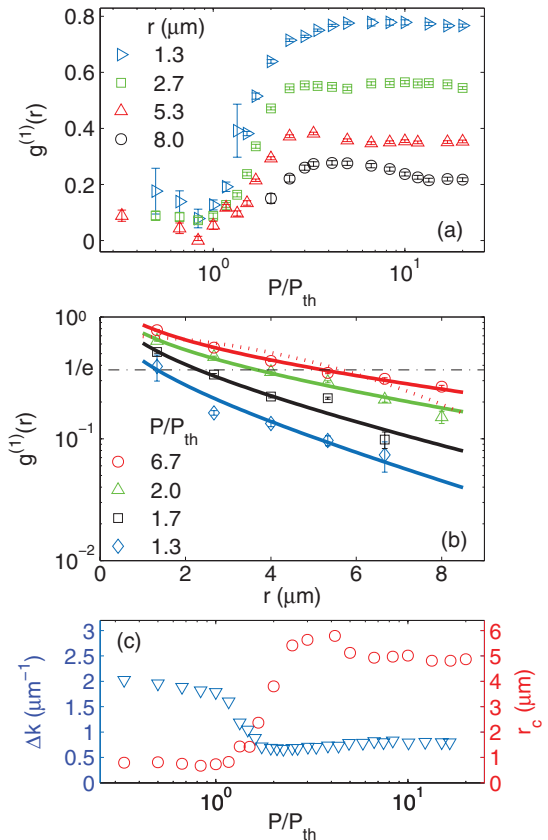

FIG. 3 (color). (a) $g^{(1)}(r)$ vs P/P_{th} for different slit separations r as labeled in the figure. (b) $g^{(1)}(r)$ vs r for different pump rates P/P_{th} as given in the legend. The symbols are measured $g^{(1)}(r)$. The solid lines are fittings by Eq. (3). The dashed line at $P/P_{th} = 7$ is a fitting by Eq. (2). The dash-dotted line marks where $g^{(1)}(r) = 1/e$. (c) r_c, the $1/e$ decay length of $g^{(1)}(r)$, vs P/P_{th} (circles) and Δk vs P/P_{th} (triangles).

the laser pump spot size of $\sim 8~\mu$m. When the pump spot size was increased to $\sim 20~\mu$m, $g^{(1)}(r) > 0.3$ was also observed up to $r = 20~\mu$m, limited again by the pump spot size [28]. This demonstrates the sudden appearance of macroscopic coherence above the condensation threshold. Another feature is that, the increase of $g^{(1)}(r)$ with P/P_{th} is slower at larger r. This shows that the macroscopic coherence is built up gradually throughout the pump beam spot size when the phase space density of LPs is increased.

To study the spatial coherence properties quantitatively, we plot in Fig. 3(b) how $g^{(1)}(r)$ decays with r, and define a coherence length r_c as $g^{(1)}(r_c) = 1/e$. The normalized pump power dependence of r_c is shown in Fig. 3(c). As a reference, for a classical Maxwell-Boltzmann (MB) gas in thermal equilibrium:

$$g^{(1)}(r) = e^{-\pi r^2/\Lambda_T^2}, \qquad r_c = \frac{\Lambda_T}{\sqrt{\pi}} = \sqrt{\frac{2\pi\hbar^2}{mk_BT}}. \qquad (2)$$

Here Λ_T is the thermal de Broglie wavelength, m is the mass of the particles, and T is temperature. For the current system at $T = 4$ K, $\Lambda_T/\sqrt{\pi} \approx 1.9~\mu$m.

Below condensation threshold density, we measured a $r_c < \Lambda_T/\sqrt{\pi}$, since the system is far from thermal equilibrium. In fact, the finite $g^{(1)}(r) \sim 0.15$ at $r = 1.3~\mu$m is consistent with the intrinsic coherence length $\xi_0 \approx 1~\mu$m of a single LP due to its finite lifetime [25]: $g_0^{(1)}(r) = \exp(-\frac{r^2}{\xi_0^2}) = 0.19$. Above condensation threshold, we found $r_c \gg \Lambda_T/\sqrt{\pi}$. Fitting of the data with Eq. (2) with temperature T as a free parameter also fails to describe the data [dashed lines in Fig. 3(b)].

Since $g^{(1)}(r)$ is the Fourier transform of the momentum distribution $f(k)$, we resort to the actual momentum distribution of the system. It was found that above the condensation threshold, the LPs become highly degenerate in the states with the lowest kinetic energies (e.g., Fig. 2 in Ref. [12]). Their momentum distribution deviates from the MB distribution, but follows well the Bose-Einstein (BE) distribution with chemical potential $|\mu| \ll k_BT$. In this quantum degenerate limit, $f(E \sim k_BT) = [\exp(\frac{E-\mu}{k_BT}) - 1]^{-1} \approx (e-1)^{-1} \ll f(0) \approx k_BT/\mu$, most of the emission comes from LPs with $E \sim 0$. Hence we can obtain the following approximate form of $g^{(1)}(r)$:

$$g^{(1)}(r) \propto \mathcal{F}^{(2D)}(f(k)g(k)) \propto \mathcal{H}(f(k)) \approx \mathcal{H}\left(\frac{k_BT}{E(k)-\mu}\right)$$

$$\propto K_0\left(r\frac{\sqrt{4\pi|\mu|/k_BT}}{\Lambda_T}\right). \qquad (3)$$

Here k is the LP's in-plane wave number, $g(k)$ is the constant momentum density of state, $\mathcal{F}^{(2D)}(f(k))$ and $\mathcal{H}(f(k))$ denote the 2D Fourier and Hankel transform of $f(k)$, respectively. As shown in Fig. 3(b) (solid lines), $K_0(x)$, the modified Bessel function of the first kind, fits very well the measured $g^{(1)}(r)$ for $P/P_{\text{th}} > 1$.

If we extrapolate the $e^{-\pi}$ decay length of $g^{(1)}(r)$ from the fitting and compare it to Λ_T at 4 K, it is $2.5\Lambda_T$ at $P = 1.2P_{\text{th}}$, and $7.9\Lambda_T$ at $P = 6.7P_{\text{th}}$.

In Fig. 3(c), we compare the pump rate dependence of r_c and Δk, the $1/e$ width of the measured first-order coherence function $g^{(1)}(r)$ and the measured momentum distribution function $f(k)$, respectively. At pump rates lower than the condensation threshold, r_c is $\sim 1~\mu$m, limited by the intrinsic coherence length ξ_0 of a single LP, while Δk is $\sim 2~\mu$m^{-1} due to the slow energy relaxation dynamics of the LPs. The product $r_c\Delta k$ is close to 2, the value expected for a thermal MB distribution. When P increases toward P_{th}, more injected LPs relax to the lower energy states and Δk gradually narrows, but r_c is still limited by ξ_0, hence a decrease in $r_c\Delta k$. Once above the threshold, there is a sudden increase of r_c by more than fivefold up to $\sim 6~\mu$m, which manifests the spontaneous buildup of a global phase among the LPs due to the phase coherent stimulated scattering of LPs into the ground state. Correspondingly, Δk is reduced by about fourfold since the LPs form a quantum degenerate Bose gas. Further increasing the pump rates, r_c decrease slightly while the momentum distribution is broadened, potentially because stronger LP-LP scattering at high densities introduces condensate dephasing [19].

Finally, it is instructive to compare Δk with the measured condensate size [9]. We have consistently observed an abnormally slow increase of the condensate size in comparison to the spot size of a photon laser based on electron-hole pairs (Fig. 6C in Ref. [9]).

Because of the discrete jump in quantum efficiency at the condensation threshold (Fig. 1 in Ref. [9]), the emission in a condensate region is much brighter. Since the pump beam has a Gaussian spatial profile, the center of the spot reaches a threshold first, leading to a sharp decrease of the emission spot size at P_{th}, for both a LP condensation and a photon laser. At $P > P_{\text{th}}$, the emission spot size measures the area which reaches the threshold. In a photon laser, threshold density is determined by the local density of electron-hole pairs independent of the system size. Hence the $1/e$ spot size ω can be estimated as:

$$\omega(P/P_{\text{th}}) = \omega_p\sqrt{1 - \log_2\left(1 + \frac{P_{\text{th}}}{P}\right)}, \qquad (4)$$

where ω_p is the pump spot size. Equation (4) describes very well the photon laser data (Fig. 6C in Ref. [9]), but fails to explain the data of a LP condensate [Ref. [9] and Fig. 4(a)]. Here we propose that for a LP condensate, $\omega(P/P_{\text{th}})$ reflects the size of the condensate in which a condensation threshold is satisfied. Then the critical LP density $n_c(\omega)$ increases with the system size ω, and the pumping rate P/P_{th} needs to be modified as $\frac{P}{P_{\text{th}}}\frac{n_c(\omega_c)}{n_c[\omega(P/P_{\text{th}})]}$, where ω_c is the condensate size at $P = P_{\text{th}}$. As a simplified model, consider n_c for a 2D boson gas confined in a finite size $L = 2\omega$ [29]: $n_c(\omega) = \frac{2}{\Lambda_T^2}\ln(\frac{2\omega}{\Lambda_T})$, then we obtain:
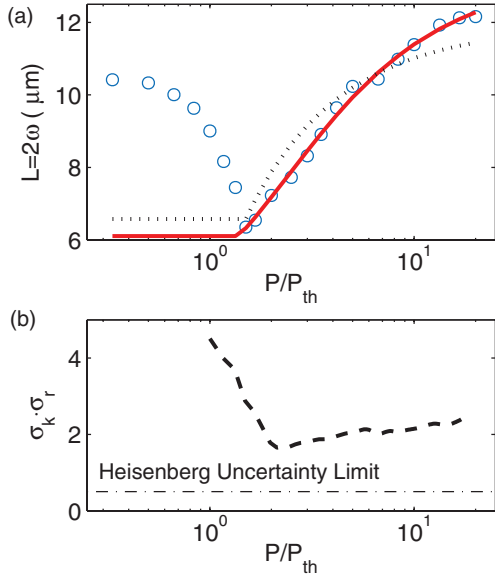
FIG. 4 (color). (a) System size 2ω vs pump rates P/P_{th}.
Symbols are the data. The solid line is a fitting by Eq. (5),
with $\omega_p = 13.3 \pm 0.1$ μm, $\omega_c = 6.1 \pm 0.1$ μm. The dotted
line is a fitting by Eq. (4) for comparison, with $\omega_p = 11.9 \pm 0.2 \mu$m. (b) The position and momentum uncertainty product
$\sigma_k \sigma_r$ vs P/P_{th}. The dash-dotted line indicates the minimum
uncertainty of $\sigma_k \sigma_r = 1/2$.

$$\omega(P/P_{th}) = \omega_p \sqrt{1 - \log_2\left(1 + \frac{P_{th}}{P}\frac{\ln(2\omega/\Lambda_T)}{\ln(2\omega_c/\Lambda_T)}\right)}. \quad (5)$$

Equation (5) fits the data very well [solid line in Fig. 4(a)],
with ω_p and ω_c as fitting parameters. This suggests that 2ω
measures the size of the coherent condensate above
threshold.

With the distribution functions in both spatial and mo-
mentum domains, we can evaluate how well the system can
be described by a single-particle wave function. The stan-
dard deviation σ_k and σ_r are calculated from the momen-
tum and spatial distribution data $f(k)$ and $f(r)$ at $P > P_{th}$,
respectively; their product is compared to the Heisenberg
minimum uncertainty limit in Fig. 4(b). The sharp decrease
of $\sigma_k \sigma_r$ at $P \sim P_{th}$ indicates that a large number of the LPs
in the system condense into a single quantum state.
Deviation from the Heisenberg limit shows that there are
some thermal LPs coexisting with the coherent condensate.
The slight increase of $\sigma_k \sigma_r$ at $P/P_{th} > 1$ may be caused by
condensate depletion due to LP-LP interactions at high
densities [19,30].

In conclusion, we studied the spatial coherence of a
microcavity polariton condensate. Young's double-slit
setup is implemented to measure the first-order coherence
function $g^{(1)}(r)$ of the LPs. The system acquires macro-
scopic coherence above a condensation threshold, mani-
fested as a sudden jump of $g^{(1)}(r)$. The observed $g^{(1)}(r)$ vs r
is well described by the Fourier transform of a degenerate
Bose-Einstein distribution in the momentum space. The

coherent condensate expands from the central region of the
pump spot to the full pump spot size, and a slow growth of
the condensate size is well understood by a simple model
of quasi-BEC with a finite size. We also confirm the
position and momentum uncertainty product $\sigma_k \sigma_r$ of the
LPs decreases toward the Heisenberg uncertainty limit
above a condensation threshold.

*Current address: Norman Bridge Laboratory of Physics
12-33, California Institute of Technology, Pasadena, CA
91125, USA
[1] O. Penrose and L. Onsager, Phys. Rev. **104**, 576 (1956).
[2] M. R. Andrews et al., Science **275**, 637 (1997).
[3] I. Bloch, T. W. Hänsch, and T. Esslinger, Nature (London) **403**, 166 (2000).
[4] Z. Hadzibabic et al., Nature (London) **441**, 1118 (2006).
[5] L. S. Dang et al., Phys. Rev. Lett. **81**, 3920 (1998).
[6] P. Senellart and J. Bloch, Phys. Rev. Lett. **82**, 1233 (1999).
[7] R. Huang et al., Phys. Rev. B **65**, 165314 (2002).
[8] H. Deng et al., Science **298**, 199 (2002).
[9] H. Deng et al., Proc. Natl. Acad. Sci. U.S.A. **100**, 15 318 (2003).
[10] M. Richard et al., Phys. Rev. Lett. **94**, 187401 (2005).
[11] J. Kasprzak et al., Nature (London) **443**, 409 (2006).
[12] H. Deng et al., Phys. Rev. Lett. **97**, 146402 (2006).
[13] P. Littlewood et al., J. Phys. Condens. Matter **16**, S3597 (2004), and refereces therein.
[14] J. Keeling et al., Semicond. Sci. Technol. **22**, R1 (2007).
[15] G. Malpuech et al., Semicond. Sci. Technol. **18**, S395 (2003).
[16] K. Kavokin et al., Phys. Rev. Lett. **92**, 017401 (2004).
[17] H. T. Cao et al., Phys. Rev. B **69**, 245325 (2004).
[18] T. D. Doan et al., Phys. Rev. B **72**, 085301 (2005).
[19] D. Sarchi and V. Savona, Phys. Rev. B **75**, 115326 (2007).
[20] A. Baas et al., Phys. Rev. Lett. **96**, 176401 (2006).
[21] N. D. Mermin and H. Wagner, Phys. Rev. Lett. **17**, 1133 (1966); **17**, 1307(E) (1966).
[22] P. Hohenberg, Phys. Rev. **158**, 383 (1967).
[23] V. Bagnato and D. Kleppner, Phys. Rev. A **44**, 7439 (1991).
[24] J. Lauwers, A. Verbeure, and V. A. Zagrebnov, J. Phys. A **36**, L169 (2003).
[25] ξ_0 of a single LP is defined by the Fourier transform of the LP's far-field radiation pattern and calculated by a transfer matrix method. A detailed procedure is given in G. Bjork et al., Phys. Rev. A **44**, 669 (1991).
[26] M. Borns and E. Wolf, *Principles of Optics* (Cambridge University Press, Cambridge, England, 1997).
[27] The operational threshold is defined at the steepest slope of the input-output curve for LPs at $k = 0$.
[28] Chih-Wei Lai et al. (to be published).
[29] W. Ketterle and N. J. van Druten, Phys. Rev. A **54**, 656 (1996).
[30] C. Orzel et al., Science **291**, 2386 (2001).